Nonlinear Dyn (2017) 87:755–766
DOI 10.1007/s11071-016-3073-x

ORIGINAL PAPER

Hopf bifurcation control of the M–L neuron model with type I

Chunli Huang · Wen Sun · Zhigang Zheng · Jinhu Lu · Shihua Chen

Received: 22 May 2016 / Accepted: 6 September 2016 / Published online: 19 September 2016

Abstract Many neurological diseases are known to be caused by bifurcations induced by a change in the values of one or more regulating parameter of nervous systems. The bifurcation control may have potential applications in the diagnosis and therapy of these dynamical diseases. In this paper, a washout filter-aided dynamic feedback controller composed of the linear term and the nonlinear cubic term is employed to control the onset of Hopf bifurcation in the Morris–Lecar (M–L) neuron model with type I. It is shown that the linear term determines the location of the Hopf bifurcation, while the nonlinear cubic term regulates the criticality of the Hopf bifurcation, preventing it from occurring in a certain range of the externally applied current. The relationships among the externally applied current, the linear control gain and the reciprocal of the filter time constant are further systematically analyzed, which help to make the best choice from the feasible parameter space to achieve our control task. Simulation results are provided to illustrate the effectiveness of the proposed methods.

Keywords Morris–Lecar model · Hopf bifurcation control · Washout filter · Neural diseases

C. Huang · W. Sun (✉)
School of Information and Mathematics, Yangtze University, Jingzhou 434023, People's Republic of China
e-mail: sunwen_2201@163.com

Z. Zheng
College of Information Science and Engineering, Huaqiao University, Xiamen 361021, People's Republic of China

J. Lu
Academy of Mathematics and Systems Science, CAS, Beijing 100190, People's Republic of China

J. Lu
The Faculty of Engineering, King Abdulaziz University, Jeddah, Saudi Arabia

S. Chen
College of Mathematics and Statistics, Wuhan University, Wuhan 430072, People's Republic of China

1 Introduction

It is well known that neural systems are complex nonlinear dynamical systems. As basic function units in neural systems, neurons can realize some functions such as responding to stimulation and conducting of excitation [1]. Through firing activity of neurons characterized by the relaxation oscillation process of producing and transmitting action potential, the information is encoded, transmitted, and decoded in the neural signal process. Many well-known neuron models such as the Morris–Lecar (M–L) model [2], Hodgkin–Huxley (H–H) model [3,4], Fitzhugh–Nagumo (F–H–N) model [5], Wilson–Cowan (W–C) model [6], and Hindmarsh–Rose (H–R) model [7], have been proposed to understand real nervous systems.

Neurodynamics has been extensively investigated on these neuron models, especially rhythmic motor behaviors, bursting [8], synchronization [9], biological function of autapse on isolate neuron and neuronal network [10], and emitting waves in network with autapses [11]. Autapses, which provide self-delayed feedback,

play an authentic physiological role in the nervous system [12]. Autapses in nature can cause many dynamic behaviors in neurons such as adjusting the response, the mode-locking status and the firing frequency and interspike interval distributions of the response spike train [13,14]. Recently, a new presented neuron models with electromagnetic induction is considered, and multiple modes of electric activities can be observed by changing the initial state [15].

Neural disorders such as Alzheimer's disease, Epilepsy [16], Parkinson's disease and schizophrenia can be interpreted as dynamical diseases. From the viewpoint of nonlinear dynamical systems, these dynamical diseases are caused by bifurcations induced by a change in the values of one or more regulating parameter of nervous systems [4]. Therefore, the understanding of these bifurcation mechanism and avoiding the occurrence of bifurcations within a certain range of parameters are of great significance for finding better treatments to such dynamical diseases.

Due to its potential applications in the diagnosis and therapy of neurological diseases, bifurcation control has become an ongoing active area of research [17]. It focuses on modifications of bifurcation characteristics of a parameterized nonlinear system by a designed control input to obtain some desired dynamical behavior or to avoid undesirable instability around bifurcations. The modifications include delaying or advancing the onset of an inherent bifurcation, modifying the shape or type of a bifurcation chain, introducing a new bifurcation at a preferable parameter value and so on. A lot of bifurcation control approaches such as static state feedback [18], frequency domain approach [19], dynamic state feedback [20], time-delayed feedback [21–23], and harmonic balance approximation [24] have been introduced in the literature.

The Hopf bifurcation control has been paid special attention for which corresponds to a concept "depolarization block" in the treatment of Schizophrenia. Grace et al. showed that dopamine-cell depolarization block provided a potential mechanism to account for their therapeutic impact on a dysregulated dopamine system [25]. Dovzhenok and Kuznetsov prepared a theoretical basis that bistability at the depolarization block should be very common among neurons [26]. We also refer the reader to the literature for details in [27]. Very recently, a dynamic state-feedback control law incorporating a washout filter [28] has been proposed, and the advantage of this control law is to preserve all the system's equilibria [29]. The washout filter-aided feedback has been successful applied to control the Hopf bifurcation in the M–L neuron model with type II [2,30,31]. However, Hopf bifurcation control of the M–L neuron model with type I excitability was neglect. In addition, most works only considered the effect of the control gain on the location of the Hopf bifurcations, and seldom took into account the relationships between the reciprocal of the filter time constant and the applied externally current or the linear control gain.

Motivated by these, in this paper, we use the washout filter-aided dynamic feedback controller to modify the bifurcation characteristics of the M–L neuron model with type I, avoiding its bifurcations to appear in a certain range of applied current. The washout filter-aided dynamic feedback controller is linear-plus-nonlinear feedback in which the linear term relocates the location of the Hopf bifurcation to an desired position, while the nonlinear cubic term regulates the criticality of the Hopf bifurcation when the linear control gain and the reciprocal of the filter time constant are appropriately selected. Moreover, the relationships among the reciprocal of the filter time constant, the applied externally current and the linear control gain are further systematically analyzed, which help to make the best choice from the feasible parameter space to achieve our control task.

The rest of this paper is organized as follows. In Sect. 2, the M–L neuron model with type I is recalled, and the conditions for the emergence of Hopf bifurcations are reviewed. In Sect. 3, the dynamic state-feedback control law incorporating a washout filter was applied to the M–L neuron model with type I. Conclusions are given in Sect. 4.

2 Preliminaries

2.1 Model description

The M–L neuron model is a biological neuron model developed to reproduce the variety of oscillatory behavior in relation to Ca^{++} and K^{+} conductance in the giant barnacle muscle fibers [32]. This model is a two-dimensional system of nonlinear differential equations:

$$\frac{dV}{dt} = \frac{1}{C}\{I - g_L(V - V_L) - g_{Ca}M_{ss}(V - V_{Ca}) - g_K N(V - V_K)\}, \quad (1)$$

$$\frac{dN}{dt} = \phi \frac{N_{ss} - N}{\tau_N}, \tag{2}$$

where

$$M_{ss} = \frac{1}{2}\left(1 + \tanh\left(\frac{V - V_1}{V_2}\right)\right),$$
$$N_{ss} = \frac{1}{2}\left(1 + \tanh\left(\frac{V - V_3}{V_4}\right)\right),$$
$$\tau_N = 1/\cosh\left(\frac{V - V_3}{2V_4}\right).$$

M_{ss}, N_{ss} and τ_N are, respectively, the voltage-dependent, the steady-state value of the recovery variable, and the time constant. V is the membrane potential, and N is the recovery variable. I is the externally applied current, and C is the membrane capacitance. V_K, V_{Ca}, V_L are the reversal potentials of the potassium, calcium, and leak currents, and g_K, g_{Ca}, g_L are the maximum conductances of the corresponding ionic currents. V_1, V_2, V_3, V_4 are constant potentials, and ϕ is the temperature factor.

2.2 The Hopf bifurcation of M–L neuron model with type I

As we said before, when the parameter changes, neuron can exhibit a bifurcation-a transition from one qualitative type of dynamics to another. There are several kinds of bifurcations such as saddle-node bifurcation, SNIC(saddle-node on invariant circle) bifurcation, and Hopf bifurcation common in the field, which are determined by the eigenvalues of the Jacobian matrix at the equilibrium [33]. Hodgkin classified neurons into three types, type I excitability, type II excitability, and type III excitability. A neuron with type I excitability starts firing at an arbitrary low frequency which is observed when the rest potential (quiescent state) disappears through a SNIC(saddle-node on invariant circle) bifurcation [30]. The experimental observation of type I can be found in [34–36]. A neuron with type II excitability begins firing at a nonzero frequency, which is observed when the rest potential loses stability via a Hopf bifurcation. While a neuron with type III excitability occurs through a quasi-separatrix crossing [37,38].

In this paper, we will focus on the M–L neuron model with type I, where I is the free parameter, the other parameter values are $C = 20\,\mu F/cm^2$, $g_L = 2.0$, $g_{Ca} = 4$, $g_K = 8.0\,mS/cm^2$, $V_L = -60$, $V_{Ca} = 120$, $V_K = -84$, $V_1 = -1.2$, $V_2 = 18$, $V_3 = 12$, $V_4 = 17.4\,mV$, and $\phi = 1/15$. The bifurcation diagram of the membrane potential V versus the externally applied current I is depicted in Fig. 1 when the externally applied current as a bifurcation parameter. The thick solid lines represent stable equilibrium points; the dotted lines represent unstable equilibrium. Filled circles represent stable periodic orbits, and open circles are unstable. Note that the bifurcation diagrams in this paper were produced using the XPPAUT software package [39] and MATLAB. The phase diagrams for the M–L neuron model with type I corresponding to the vertical dashed lines in Fig. 1 are plotted in Fig. 2. When $I = -30\,\mu A/cm^2$, the M–L neuron model has a SEP (stable equilibrium point) which can be seen from Fig. 2a. By increasing I to $I = 0\,\mu A/cm^2$, three equilibrium points are generated, and one of them is stable which is shown in Fig. 2b. When increasing I to $I = 39.96\,\mu A/cm^2$, it undergoes a SNIC bifurcation from quiescence to periodic spiking [33]—an abrupt and transient change of membrane voltage that propagates to other neurons via an axon illustrated in Fig. 2c. After the SNIC bifurcation point, there emerge a SLC (stable limit cycle) and an UEP (unstable equilibrium point) at $I = 70\,\mu A/cm^2$ in Fig. 2d. By further increasing I, there is a subcritical HB (Hopf bifurcation) at

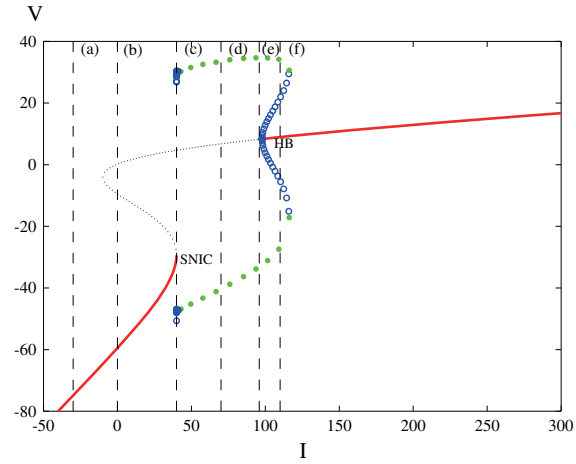

Fig. 1 Bifurcation diagram for the M–L neuron model with type I. The *thick solid lines* represent stable equilibrium points, and the *dotted lines* represent unstable equilibrium. *Filled circles* represent stable periodic orbits and *open circles* are unstable. The *vertical dashed lines* represent $I = -30$, $I = 0$, $I = 39.96$, $I = 70$, $I = 97.79$, $I = 110\,\mu A/cm^2$, respectively

$I = 97.79\,\mu\text{A/cm}^2$ from unstable state to stable state which is generically orbitally asymptotically unstable shown in Fig. 2e. After this subcritical Hopf bifurcation point, there appears a stable equilibrium point and two limit cycles, one of which is stable, namely, there is a bistability. An example of the bistability at $I = 110\,\mu\text{A/cm}^2$ is illustrated in Fig. 2f.

2.3 Conditions for emergence of Hopf bifurcations

Let

$$\frac{\mathrm{d}x}{\mathrm{d}t} = f_\mu(x, u) \tag{3}$$

where $x \in R^n$ is the state vector, $\mu \in R$ is the bifurcation parameter, $f_\mu(x, u)$ is a smooth map from $R^n \times R$ to R^n and u is a scalar input. Assume that there is a fixed point x_μ for the parameter value μ, with eigenvalues $\lambda_\mu = \alpha_\mu + i\beta_\mu$. Suppose that $\beta_\mu \neq 0, \alpha_{\mu_0} = 0$, and $\frac{\mathrm{d}}{\mathrm{d}\mu}(\alpha_\mu)|_{\mu=\mu_0} > 0$, then there is a Hopf bifurcation in the parameter value $\mu = \mu_0$.

In some systems especially in high-dimensional system, the eigenvalues cannot always be obtained. In order to avoid this kind of situation, we can use the equivalent conditions for the emergence of Hopf bifurcation based on the Routh–Hurwitz stability criterion [40]. Suppose the characteristic polynomial of the Jacobian matrix be

$$p(\lambda, \mu) = p_0(\mu) + p_1(\mu)\lambda + \cdots + p_n(\mu)\lambda^n. \tag{4}$$

Let

$$L_n(\mu) = \begin{pmatrix} p_1(\mu) & p_0(\mu) & \cdots & 0 \\ p_3(\mu) & p_2(\mu) & \cdots & 0 \\ \vdots & \vdots & \ddots & \vdots \\ p_{2n-1}(\mu) & p_{2n-2}(\mu) & \cdots & p_n(\mu) \end{pmatrix}, \tag{5}$$

where $p_i(\mu) = 0$, if $i < 0$ or $i > n$. Assume

$$D_1(\mu) = \det(L_1(\mu)) = p_1(\mu), \tag{6}$$

$$D_2(\mu) = \det(L_2(\mu)) = det \begin{pmatrix} p_1(\mu) & p_0(\mu) \\ p_3(\mu) & p_2(\mu) \end{pmatrix}, \tag{7}$$

$$\cdots$$

$$D_n(\mu) = \det(L_n(\mu)). \tag{8}$$

According to [40], system (3) undergoes a Hopf bifurcation at $\mu = \mu_0$ satisfies the following condition:

(a): $p_0(\mu_0) > 0$, $D_1(\mu_0) > 0$, …, $D_{n-2}(\mu_0) > 0$, $D_{n-1}(\mu_0) = 0$;

(b): $\frac{dD_{n-1}(\mu)}{\mathrm{d}\mu}|_{\mu=\mu_0} \neq 0$.

3 Controlling the M–L neuron model with type I

3.1 The dynamic state-feedback control law

A dynamic state-feedback control law based on washout filters [41] for controlling Hopf bifurcations in system (3) is introduced as follows

$$\frac{\mathrm{d}x}{\mathrm{d}t} = f_\mu(x) + u(x, y), \tag{9}$$

$$\frac{\mathrm{d}y_i}{\mathrm{d}t} = x_i - d_i y_i, i = 1, \ldots, m, \tag{10}$$

$$u_i(x_i, y_i) = -k_{1i}(x_i - d_i y_i) - k_{3i}(x_i - d_i y_i)^3, \tag{11}$$

where $u(x, y) = [u_1(x_1, y_1), \ldots, u_m(x_m, y_m), 0, \ldots, 0]^T$, k_{1i} and k_{3i} are the control gains, and d_i is the reciprocal of the filter time constant. When $k_{1i} \neq 0$ and $k_{3i} = 0$, the controller just a linear controller. When $k_{1i} = 0$ and $k_{3i} \neq 0$, the controller is a nonlinear controller. While $k_{1i} \neq 0$ and $k_{3i} \neq 0$, it is a combined linear-plus-nonlinear feedback controller.

Because the membrane potential V is readily measured, we only select it as the input to be controlled. The controlled M–L neuron model with type I is given:

$$\frac{\mathrm{d}V}{\mathrm{d}t} = \frac{1}{C}\{I - g_\mathrm{L}(V - V_\mathrm{L}) - g_\mathrm{Ca}M_\mathrm{ss}(V - V_\mathrm{Ca}) - g_\mathrm{K}N(V - V_\mathrm{K})\} - k_1(V - \mathrm{d}y) - k_3(V - \mathrm{d}y)^3, \tag{12}$$

$$\frac{\mathrm{d}N}{\mathrm{d}t} = \phi\frac{N_\mathrm{ss} - N}{\tau_N}, \tag{13}$$

$$\frac{\mathrm{d}y}{\mathrm{d}t} = V - \mathrm{d}y. \tag{14}$$

3.2 The linear feedback controller

When $k_3 = 0$, $k_1 \neq 0$, this controller is just a linear feedback controller. We firstly advance the Hopf bifurcation to $I_1 = 70\,\mu\text{A/cm}^2$ when $d = 1$. In order to achieve our goal, we get the value of the control gain k_1 using the Routh–Hurwitz stability criterion [40].

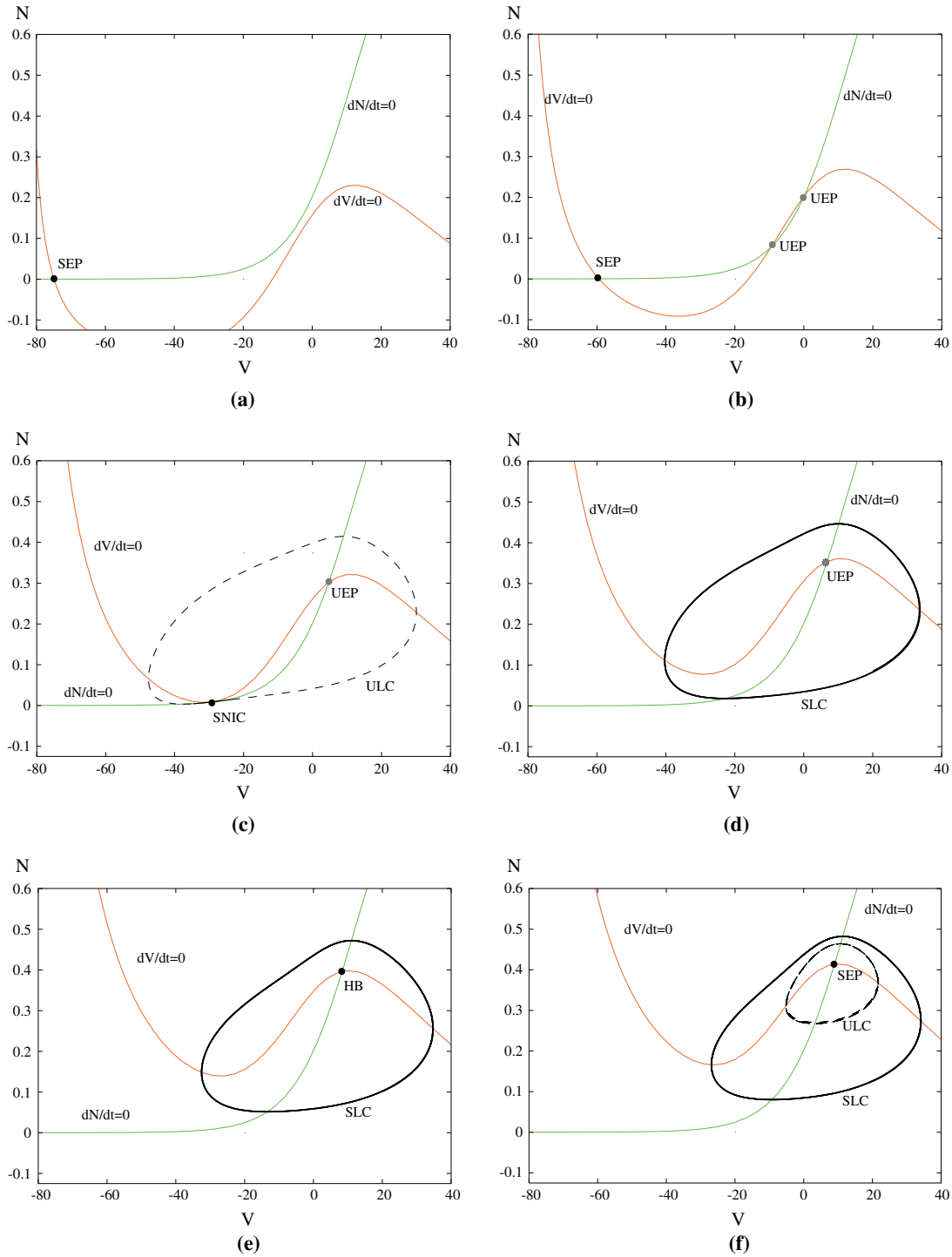

Fig. 2 Phase diagrams for the M–L neuron model with type I under different externally applied current I corresponding to the *vertical dashed lines* in Fig. 1. **a** $I = -30\,\mu\text{A/cm}^2$, **b** $I = 0\,\mu\text{A/cm}^2$, **c** $I = 39.96\,\mu\text{A/cm}^2$, **d** $I = 70\,\mu\text{A/cm}^2$, **e** $I = 97.79\,\mu\text{A/cm}^2$, **f** $I = 110\,\mu\text{A/cm}^2$. The *thick solid* and *dotted closed curves* denote stable limit cycles (SLC) and unstable limit cycles (ULC), respectively. *Red* and *green solid lines* indicate V- and N-nullclines of M–L neuron model. *Black* and *gray* points indicate stable equilibrium points (SEP) and unstable equilibrium points (UEP). (Color figure online)

At $I_1 = 70\,\mu\text{A/cm}^2$, $(V_1, N_1) = (6.793, 0.3547)$, the Jacobian matrix is

$$L(I_1) = \begin{bmatrix} 0.1360 - k_1 & -36.3172 & k_1 \\ 0.0018 & -0.0674 & 0 \\ 1 & 0 & -1 \end{bmatrix}. \quad (15)$$

Then, we get the characteristic polynomial of $L(I_1)$:

$$p(\lambda, I_1) = p_0(I_1) + p_1(I_1)\lambda + p_2(I_1)\lambda^2 + p_3(I_1)\lambda^3, \quad (16)$$

where $p_0(I_1) = 0.0562$, $p_1(I_1) = 0.0674k_1 - 0.0124$, $p_2(I_1) = k_1 + 0.9314$, $p_3(I_1) = 1$.

According to the equivalent conditions for the emergence of Hopf bifurcation (a) and (b), one get

$$p_0(I_1) = 0.0562 > 0, \quad (17)$$

$$D_1(I_1) = p_1(I_1) = 0.0674k_1 - 0.0124 > 0, \quad (18)$$

$$D_2(I_1) = p_1(I_1) * p_2(I_1) - p_0(I_1) * p_3(I_1) = 0, \quad (19)$$

$$\frac{dD_2(I)}{dI}|_{I=I_1} = 1.0974 \times 10^{-6} \neq 0. \quad (20)$$

Solving the two inequalities and one equality, we obtain $k_1 = 0.6963$. Figure 3a shows the location of the Hopf bifurcation has been successfully advanced from $I = 97.79$ to $I_1 = 70\,\mu\text{A/cm}^2$. Now, we will uncover how the parameters such as the reciprocal of the filter time constant, the applied externally current and the linear control gain influence each other. When $k_1 = 0.6963$, the variation of the reciprocal of the filter time constant d changing with the externally applied current I (the location of the Hopf bifurcation point) is shown in Fig. 3b. Clearly, with the increase in the externally applied current I, the reciprocal of the filter time constant d is increasing slowly below $I = 80\,\mu\text{A/cm}^2$, and sharply over $I = 80\,\mu\text{A/cm}^2$. Therefore, the reciprocal of the filter time constant d has much effect on the location of the Hopf bifurcation point. We fix $d = 1$, the relationship between the externally applied current I and the corresponding control parameter k_1 is shown in Fig. 3c. The left straight line indicates that the location of SNIC bifurcation point does not to be transferred with changing k_1, and the curve shows k_1 will decrease slowly with the increase of the externally applied current I. At the Hopf bifurcation point $I_1 = 70\,\mu\text{A/cm}^2$, the relationship between d and k_1, i.e., k_1 will increase slowly with the increase in the reciprocal of the filter time constant d, is shown in Fig. 3d.

We also can delay the Hopf bifurcation to $I_2 = 200\,\mu\text{A/cm}^2$, where $(V_2, N_2) = (12.93, 0.5267)$. The Jacobian matrix is

$$L(I_2) = \begin{bmatrix} -0.1370 - k_1 & -38.772 & k_1 \\ 0.0019 & -0.0667 & 0 \\ 1 & 0 & -1 \end{bmatrix}. \quad (21)$$

Then, we get the characteristic polynomial of $L(I_2)$:

$$p(\lambda, I_2) = p_0(I_2) + p_1(I_2)\lambda + p_2(I_2)\lambda^2 + p_3(I_2)\lambda^3, \quad (22)$$

where $p_0(I_2) = 0.0828$, $p_1(I_2) = 0.0667k_1 + 0.2865$, $p_2(I_2) = k_1 + 1.2037$, $p_3(I_2) = 1$.

According to the equivalent conditions for the emergence of Hopf bifurcation (a) and (b), we have

$$p_0(I_2) = 0.0828 > 0, \quad (23)$$

$$D_1(I_2) = p_1(I_2) = 0.0667k_1 + 0.2865 > 0, \quad (24)$$

$$D_2(I_2) = p_1(I_2) * p_2(I_2) - p_0(I_2) * p_3(I_2) = 0, \quad (25)$$

$$\frac{dD_2(I)}{dI}|_{I=I_2} = 1.1789 \times 10^{-4} \neq 0. \quad (26)$$

Solving the two inequalities and one equality, one get $k_1 = -0.844$. Figure 4a shows the location of the Hopf bifurcation has been successfully delayed from $I = 97.79$ to $I_2 = 200\,\mu\text{A/cm}^2$. The point $I = 97.79\,\mu\text{A/cm}^2$ becomes an unstable equilibrium point. When $k_1 = -0.844$, the variation of the reciprocal of the filter time constant d changing with the externally applied current I is shown in Fig. 4b. We find that with the increase in the externally applied current I, the reciprocal of the filter time constant d is decreasing sharply below $I = 120\,\mu\text{A/cm}^2$, and slowly over $I = 120\mu\,\text{A/cm}^2$. At $I_2 = 200\,\mu\text{A/cm}^2$, the relationship between d and k_1, i.e., k_1 will decrease slowly with the increase in the reciprocal of the filter time constant d, is shown in Fig. 4c.

From Figs. 3 and 4, we can see that the location of the Hopf bifurcation point is transferred to the given point according to our requirements when the parameters are properly selected. What's more, the change of the parameters such as the reciprocal of the filter time constant and the linear control gain have nonnegligible

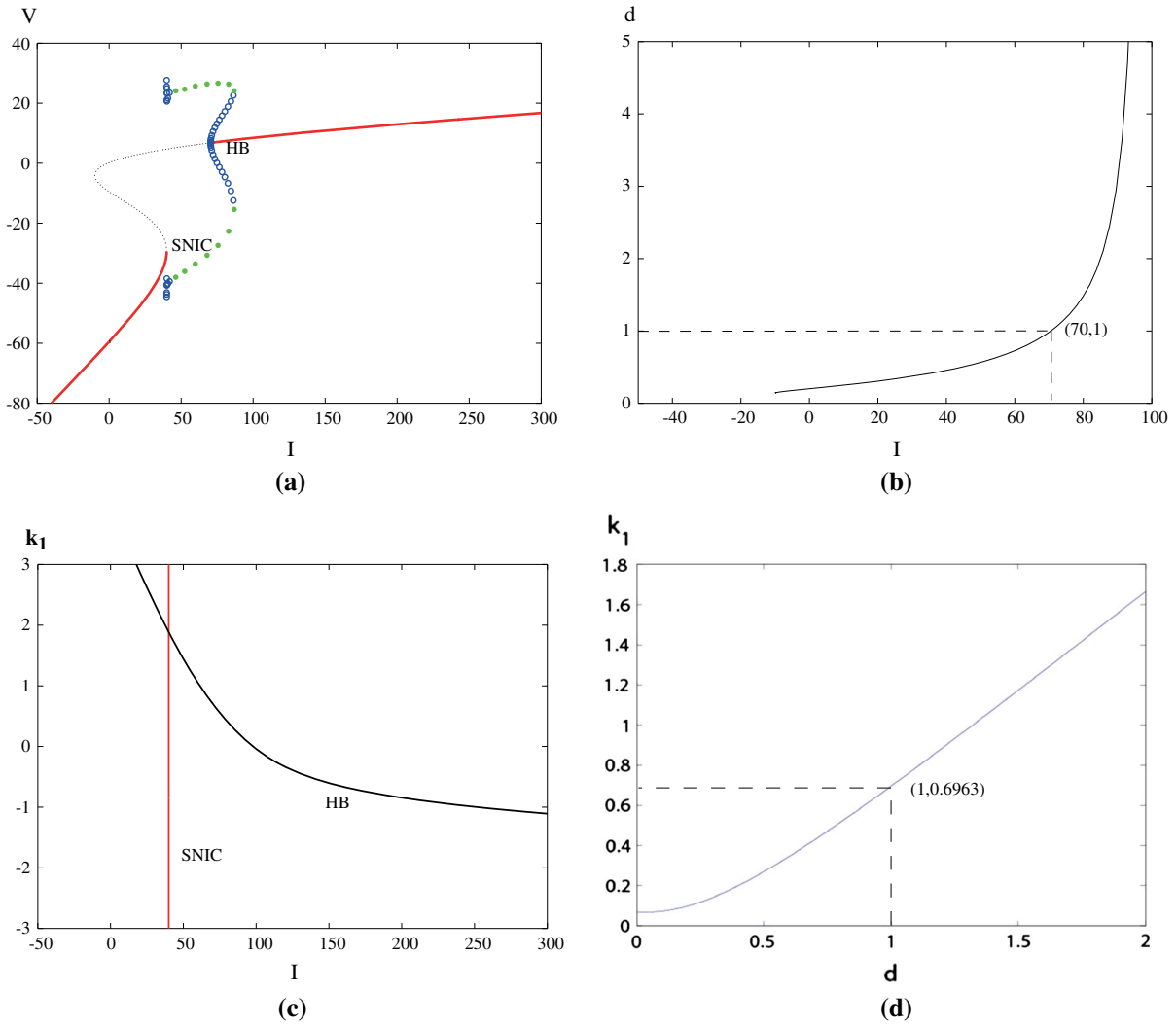

Fig. 3 **a** Bifurcation diagram of closed-loop M–L system where the inherent Hopf bifurcation has been advanced to $I_1 = 70\,\mu\text{A/cm}^2$ with $k_1 = 0.6963$. **b** Two-parameter diagram depicting I with respect to d when $k_1 = 0.6963$. **c** Two-parameter diagram depicting I with respect to k_1 when $d = 1$. **d** Two-parameter diagram depicting d with respect to k_1 at Hopf bifurcation point $I_1 = 70\,\mu\text{A/cm}^2$

influence on the Hopf bifurcation. Compared with the uncontrolled M–L neuron model, the oscillation amplitude of the bifurcated limit cycles of the controlled M–L neuron model undergoes great changes, i.e., it decreases when the Hopf bifurcation is advanced to $I_1 = 70\,\mu\text{A/cm}^2$, and increases when the Hopf bifurcation is delayed to $I_2 = 200\,\mu\text{A/cm}^2$. Since the linear feedback controller only adjusts the location of the Hopf bifurcation other than the stability of the bifurcated limit cycles, the location of the Hopf bifurcation is supposed to regulate the oscillation amplitude, i.e., the advanced Hopf bifurcation point results in the decrease in the oscillation amplitude while the delayed Hopf bifurcation point leads to the increase in the oscillation amplitude.

3.3 The nonlinear feedback controller

When $k_1 = 0, k_3 \neq 0$, this controller becomes a nonlinear feedback controller which is used to stabilize the Hopf bifurcation. Let the nonlinear feedback gain

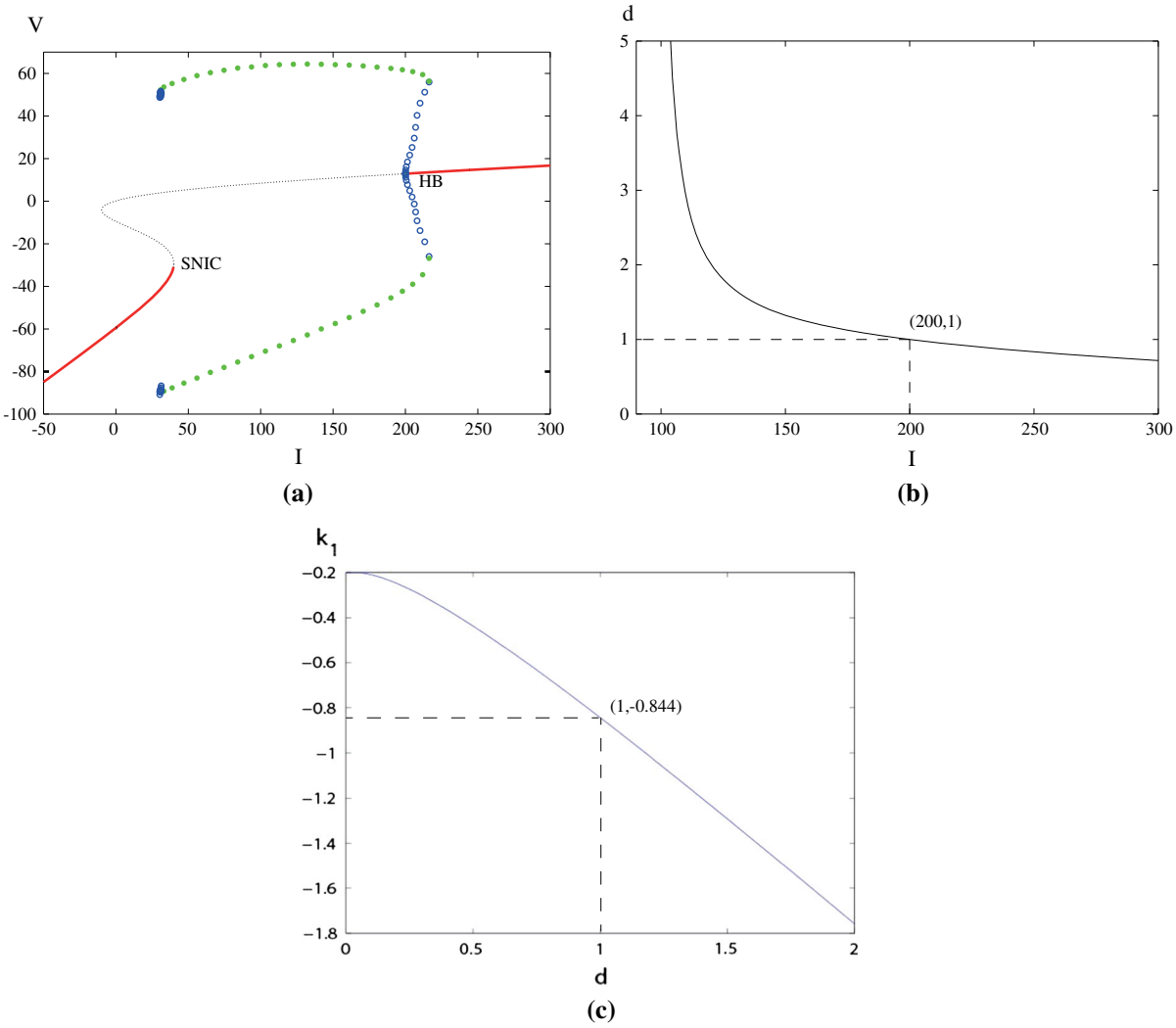

Fig. 4 **a** Bifurcation diagram of closed-loop M–L system where the inherent Hopf bifurcation has been delayed to $I_2 = 200\,\mu\text{A/cm}^2$ with $k_1 = -0.844$. **b** Two-parameter bifurcation diagram depicting continuation of Hopf bifurcation point with respect to d when $k_1 = -0.844$. **c** Two-parameter diagram depicting d with respect to k_1 at Hopf bifurcation point $I_2 = 200\,\mu\text{A/cm}^2$

$k_3 = 1.75$ and $d = 1$, Fig. 5a shows that the Hopf bifurcation remains at $I = 97.79\,\mu\text{A/cm}^2$, but the periodic orbit becomes generically orbitally asymptotically stable, which is called a supercritical bifurcation. At the same time, the oscillation amplitude of the bifurcated limit cycle decreases greatly. Namely, the unstable limit cycles are translated to reduced amplitude stable limit cycles, and the subcritical Hopf bifurcation in the uncontrolled M–L neuron model becomes supercritical Hopf bifurcation in the controlled one. We concludes that the stable bifurcated limit cycle can suppress the oscillation amplitude of the bifurcated limit cycle. When $k_1 = 0, k_3 = 1.75$, the relationship between the reciprocal of the filter time constant d and the externally applied current I is shown in Fig. 5b, which indicates that the reciprocal of the filter time constant d has no effect on the location of the Hopf bifurcation point. Figure 5c depicts the relationship between the externally applied current I and the corresponding control parameter k_3. It is obvious that the value of k_3 cannot

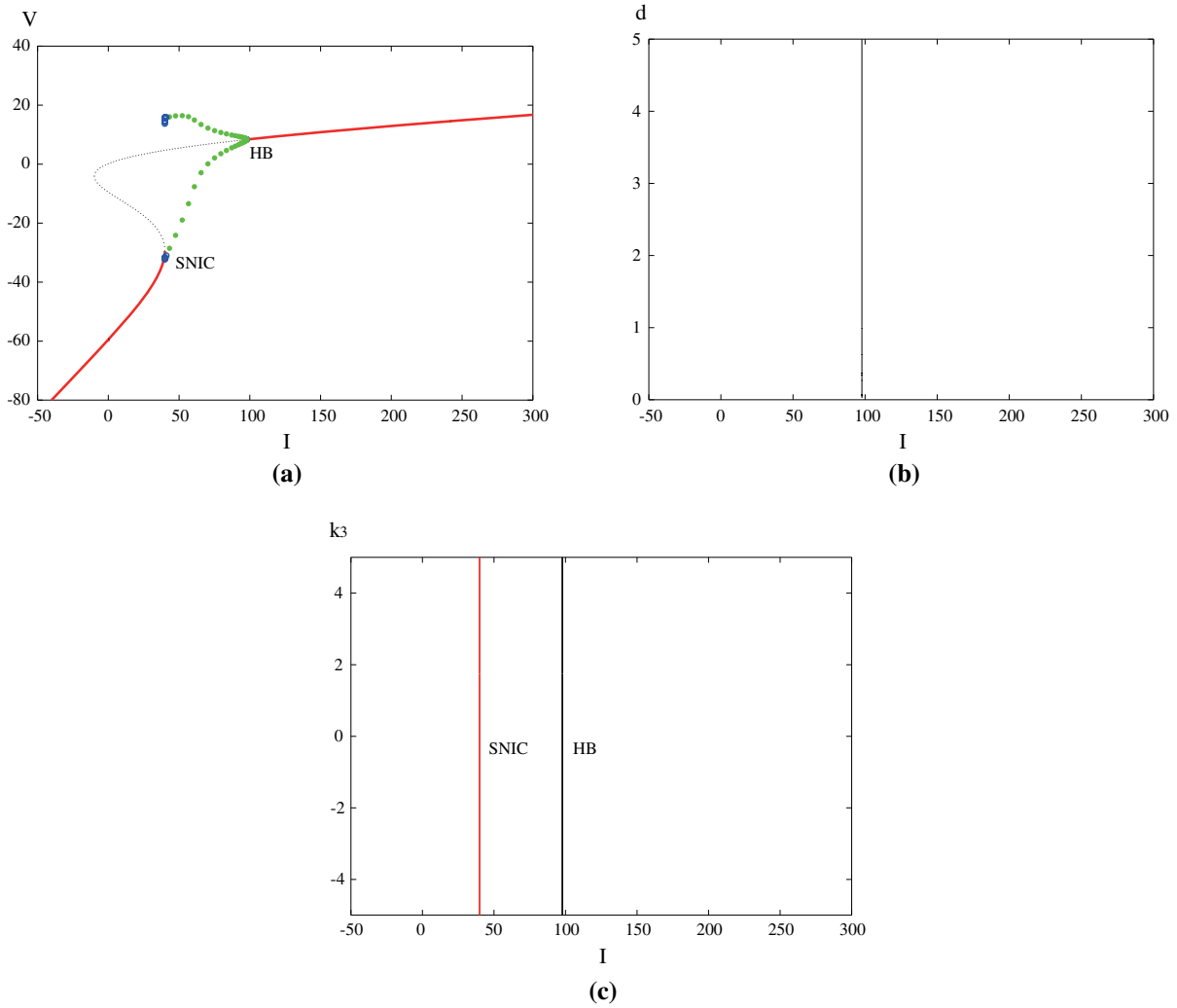

Fig. 5 **a** Bifurcation diagram of controlled M–L system with $k_1 = 0$, $k_3 = 1.75$ and $d = 1$. **b** Two-parameter bifurcation diagram depicting continuation of Hopf bifurcation point with respect to d when $k_1 = 0$, $k_3 = 1.75$. **c** Two-parameter bifurcation diagram depicting continuation of SNIC bifurcation point and Hopf bifurcation point with respect to k_3

affect the location of SNIC bifurcation point and the Hopf bifurcation point.

When $k_1 \neq 0$, $k_3 \neq 0$, the controller is a linear-plus-nonlinear feedback controller. Let $d = 1$, $k_1 = -0.844$, $k_3 = 3$, Fig. 6a shows the location of Hopf bifurcation is translated from $I = 97.79$ to $I_2 = 200\,\mu\text{A/cm}^2$, and the subcritical Hopf bifurcation is transformed into the supercritical Hopf bifurcation. In addition, the oscillation amplitude decreases greatly. We conclude that the decrease in the oscillation amplitude resulted from the stable bifurcated limit cycle is supposed to far surpasses the increase in the oscillation amplitude resulted from the delayed Hopf bifurcation point according to previous discussion. Figure 6b shows the variation of the reciprocal of the filter time constant d changing with the externally applied current I when $k_1 = -0.844$, $k_3 = 3$. The relationship between d and I is same as the case of $k_1 = -0.844$, $k_3 = 0$ in Fig. 4b, which suggests that k_3 can't affect the location of the Hopf bifurcation point. Figure 6c illustrates that the relationship between the externally applied current I and the corresponding control parameter k_1. Compared with Figs. 3c, 6c further indicates that the nonlinear part of the controller can

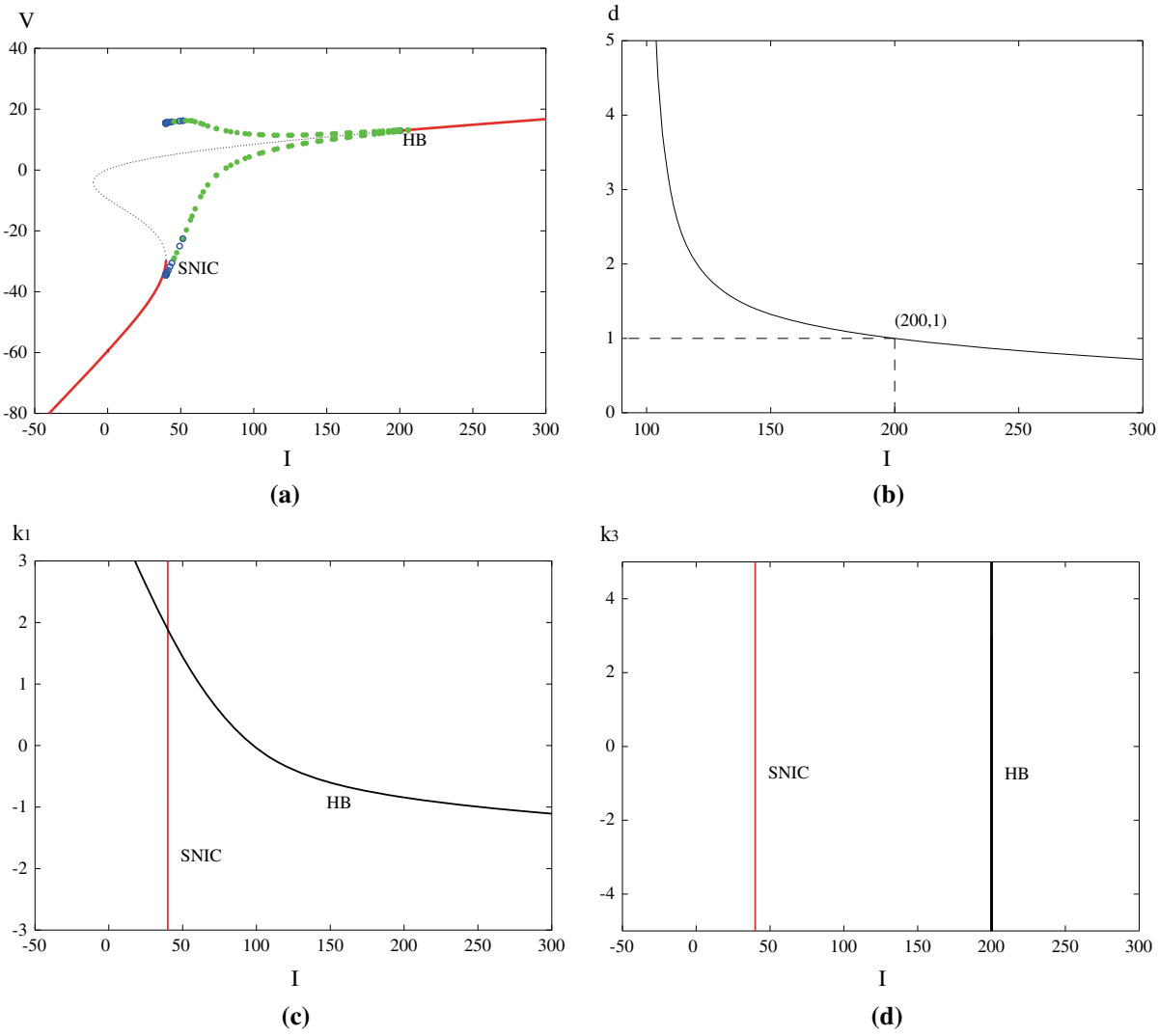

Fig. 6 **a** Bifurcation diagram of controlled M–L system in which the inherent Hopf bifurcation has been relocated to new position, the stability and the oscillation amplitude have been changed when $d = 1$, $k_1 = -0.844$, $k_3 = 3$. **b** Two-parameter bifurcation diagram depicting continuation of Hopf bifurcation point with respect to d when $k_1 = -0.844$, $k_3 = 3$. **c** Two-parameter bifurcation diagram depicting continuation of SNIC bifurcation point and Hopf bifurcation point with respect to k_1 when $d = 1$, $k_3 = 3$. **d** Two-parameter bifurcation diagram depicting continuation of SNIC bifurcation point and Hopf bifurcation point with respect to k_3 when $d = 1$, $k_1 = -0.844$

not affect the location of the Hopf bifurcation point. Figure 6d depicts the relationship between the externally applied current I and the corresponding control parameter k_3. It is obvious that k_3 can't affect the location of the Hopf bifurcation point, and only the linear part of the controller affect the location of the Hopf bifurcation point. Therefore, the linear-plus-nonlinear feedback controller can change the location of the Hopf bifurcation point by the linear part, and regulate the stability and the oscillation amplitude of the bifurcated limit cycle by the nonlinear part. The above-mentioned methods can also be applied to other complex nonlinear dynamical systems such as higher-dimensional chaotic systems [42] and multi-agent systems [43].

4 Conclusions

In this paper, we have emploied a washout filter-aided dynamic feedback controller to control the onset of

Hopf bifurcation in the M–L neuron model with type I. The linear term of the linear-plus-nonlinear feedback controller determines the location of the Hopf bifurcation, while the nonlinear cubic term regulates the criticality of the Hopf bifurcation. Therefore, the designed controller can advance or delay the Hopf bifurcation, preventing it from occurring in a certain range of the externally applied current. How the other parameters affect the location of the Hopf bifurcation point are further systematically analyzed. The proposed bifurcation control method may have potential applications in the diagnosis and therapy of neurological diseases.

Acknowledgements The work is supported by the National Key Research and Development Program of China under Grant 2016YFB0800401, the National Natural Science Foundation of China under Grants 61621003, 61532020, 11472290, 61472027, 11475022, 11547006, 61503046, the Key Program of Frontier Science of the Chinese Academy of Sciences under Grant QYZDJ-SSW-JSC003, and Guangxi Education Department Key Laboratory of Symbolic Computation and Engineering Data Processing (No. FH201502).

References

1. Dimitrov, A., Lazar, A., Victor, J.: Information theory in neuronscience. J. Comput. Neurosci. **30**(1), 1–5 (2011)
2. Nguyen, L., Hong, K.: Hopf bifurcation control via a dynamic state-feedback control. Phys. Lett. A **376**(4), 442–446 (2012)
3. Ding, L., Hou, C.: Stabilizing control of Hopf bifurcation in the Hodgkin–Huxley model via washout filter with linear control term. Nonlinear Dyn. **60**(1–2), 131–139 (2009)
4. Xie, Y., Chen, L., Kang, Y., Aihara, K.: Controlling the onset of Hopf bifurcation in the Hodgkin–Huxley model. Phys. Rev. E **77**(6), 061921 (2008)
5. Nguyen, L., Hong, K.: Synchronization of coupled chaotic FitzHugh–Nagumo neurons via Lyapunov functions. Math. Comput. Simul. **82**(4), 590–603 (2011)
6. Ueta, T., Chen, G.: On synchronization and control of coupled Wilson–Cowan neural oscillators. Int. J. Bifurc. Chaos **13**(1), 163–175 (2003)
7. Yu, H.J., Tong, W.J.: Chaotic control of Hindmarsh–Rose neuron by delayed self-feedback. Acta Phys. Sin. **58**, 2977–2982 (2009)
8. Shi, M., Wang, Z.: Abundant bursting patterns of a fractional-order Morris–Lecar neuron model. Commun. Nonlinear Sci. Numer. Simul. **19**(6), 1956–1969 (2014)
9. Wang, H., Lu, Q., Wang, Q.: Bursting and synchronization transition in the coupled modified M–L neurons. Commun. Nonlinear Sci. Numer. Simul. **13**(8), 1668–1675 (2008)
10. Ma, J., Tang, J.: A review for dynamics of collective behaviors of network of neurons. Sci. China Technol. Sci. **58**(2), 2038–2045 (2015)
11. Qin, H.X., Wu, Y., Wang, C.N., Ma, J.: Emitting waves from defects in network with autapses. Commun. Nonlinear Sci. Numer. Simul. **23**(1), 164–174 (2015)
12. Wang, H.T., Chen, Y.: Firing dynamics of an autaptic neuron. Chin. Phys. B **24**(12), 128709 (2015)
13. Yao, C., Ma, J., Li, C., He, Z.: The effect of process delay on dynamical behaviors in a self-feedback nonlinear oscillator. Common. Nonlinear Sci. Numer. Simul. **39**, 99–107 (2016)
14. Wang, H.T., Ma, J., Chen, Y.L., Chen, Y.: Effect of an autapse on the firing pattern transition in a bursting neuron. Common. Nonlinear Sci. Numer. Simul. **19**(9), 3242–3254 (2014)
15. Lü, M., Wang, C.N., Ren, G.D., Ma, J., Song, X.L.: Model of electrical activity in a neuron under magnetic flow effect. Nonlinear Dyn. **85**(3), 1479–1490 (2016)
16. Milton, J., Jung, P.: Brain defibrillators: synopsis, problems and future directions. In: Epilepsy as a Dynamic Disease. Springer, Berlin Heidelberg (2003)
17. Chen, G., Moiola, J., Wang, H.: Bifurcation control: theories, methods and applications. Int. J. Bifurc. Chaos **10**(3), 511–548 (2000)
18. Abed, E., Fu, J.: Local feedback stabilization and bifurcation control, I. Hopf bifurcation. Syst. Control Lett. **7**(1), 11–17 (1986)
19. Liao, X.F., Li, S.W., Wong, K.W.: Hopf bifurcation on a two-neuron system with distributed delays: a frequency domain approach. Nonlinear Dyn. **31**(3), 299–326 (2003)
20. Yu, P., Chen, G.R.: Hopf bifurcation control using nonlinear feedback with polynomial functions. Int. J. Bifurc. Chaos **14**(5), 1683–1704 (2004)
21. Brandt, M.E., Chen, G.R.: Bifurcation control of two nonlinear models of cardiac activity. IEEE Trans. Circuits Syst. I **44**(10), 1031–1034 (1997)
22. Jiang, J., Song, Y.L.: Delay-induced Bogdanov–Takens bifurcation in a Leslie–Gower predator-prey model with nonmonotonic functional response. Commun. Nonlinear Sci. Numer. Simul. **19**(7), 2454–2465 (2014)
23. Xiao, M., Ho, D., Cao, J.: Time-delayed feedback control of dynamical small-world networks at Hopf bifurcation. Nonlinear Dyn. **58**(1–2), 319–344 (2009)
24. Tesi, A., Abed, E., Genesio, R., Wang, H.: Harmonic balance analysis of period-doubling bifurcations with implications for control of nonlinear dynamics. Automatica **32**(9), 1255–1271 (1996)
25. Grace, A.A., Bunney, B.S., Moore, H., Todd, C.L.: Dopamine-cell depolarization block as a model for the therapeutic actions of antipsychotic drugs. Trends Neurosci. **20**(1), 31–37 (1997)
26. Dovzhenok, A., Kuznetsov, A.S.: Exploring neuronal bistability at the depolarization block. Plos One **7**(8), 324–325 (2012)
27. Gu, H.G., Pan, B.B.: Identification of neural firing patterns, frequency and temporal coding mechanisms in individual aortic baroreceptors. Front. Comput. Neurosci. doi:10.3389/fncom.2015.00108
28. Wang, H., Abed, E.: Bifurcation control of a chaotic system. Automatica **31**(9), 1213–1226 (1995)
29. Chen, Z., Yu, P.: Controlling and anti-controlling Hopf bifurcations in discrete maps using polynomial functions. Chaos Solitons Fractals **26**(4), 1231–1248 (2005)

30. Nguyen, L., Hong, K., Park, S.: Bifurcation control of the Morris-Lecar neuron model via a dynamic state-feedback control. Biol. Cybern. **106**(10), 587–594 (2012)
31. Nguyen L., Hong K.: Analysis and control of the bifurcation in a Morris–Lecar neuron via a washout filter-aided dynamic control law. In: 11th International Conference on Control, Automation and Systems (ICCAS), pp. 342–347. (2011)
32. Morris, C., Lecar, H.: Voltage oscillations in the barnacle giant muscle fiber. Biophys. J. **35**(1), 193–213 (1981)
33. Izhikevich, E.M.: Dynamical Systems in Neuroscience: The Geometry of Excitability and Bursting. MIT Press, Cambridge (2007)
34. Jia, B., Gu, H.G.: Identifying type I excitability using dynamics of stochastic neural firing patterns. Cogn. Neurodyn. **6**(6), 485–497 (2012)
35. Jia, B., Gu, H.G., Li, Y.Y.: Coherence-resonance-induced neuronal firing near a saddle-node and homoclinic bifurcation corresponding to type-I excitability. Chin. Phys. Lett. **28**(9), 90507 (2011)
36. Gu, H.G., Zhang, H.M., Wei, C.L., Yang, M.H., Liu, Z.Q., Ren, W.: Coherence resonance induced stochastic neural firing at a saddle-node bifurcation. Int. J. of Mod. Phys. B **25**(29), 3977–3986 (2011)
37. Prescott, S.A., De Koninck, Y., Sejnowski, T.J.: Biophysical basis for three distinct dynamical mechanisms of action potential initiation. PLoS Comput. Biol. **4**(10), e1000198 (2008)
38. Wang, H., Wang, L., Yu, L., Chen, Y.: Response of Morris–Lecar neurons to various stimuli. Phys. Rev. E **83**, 021915 (2011)
39. Ermentrout, B.: Simulating, Analyzing, and Animating Dynamical Systems: A Guide to XPPAUT for Researchers and Students. Society for Industrial and Applied Mathematics, Philadelphia (2002)
40. Liu, W.: Criterion of Hopf bifurcations without using eigenvalues. J. Math. Anal. Appl. **182**(1), 250–256 (1994)
41. Lee, H., Abed, E.: Washout filters in the bifurcation control of high alpha flight dynamics. In: American Control Conference, pp. 206–211. (1991)
42. Wang, Q., Yu, S., Li, C., Lü, J., Fang, X., Guyeux, C., Bahi, J.M.: Theoretical design and FPGA-based implementation of higher-dimensional digital chaotic systems. IEEE Trans. Circuits Syst. I **63**(3), 401–412 (2016)
43. Liu, K., Wu, L., Lü, J., Zhu, H.: Finite-time adaptive consensus of a class of multi-agent systems. Sci. China – Technol. Sci. **59**(1), 22–32 (2016)